Scilight

Materials and Sustainability
https://www.sciltp.com/journals/matsus

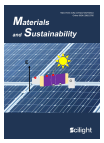

Article

Structural Phase Transitions in Double Perovskite Crystals Studied by Brillouin Light Scattering

Dmytro O. Horiachyi [1,*], Mikhail O. Nestoklon [1], Ilya A. Akimov [1], Dmitri R. Yakovlev [1], Volodymyr Vasylkovskyi [2], Olga Trukhina [2], Vladimir Dyakonov [2] and Manfred Bayer [1,3]

[1] Experimentelle Physik 2, Technische Universität Dortmund, 44227 Dortmund, Germany
[2] Experimental Physics 6 and Würzburg-Dresden Cluster of Excellence ctd.qmat, Julius Maximilian University of Würzburg, 97074 Würzburg, Germany
[3] Research Center FEMS, Technische Universität Dortmund, 44227 Dortmund, Germany
* Correspondence: dmytro.horiachyi@tu-dortmund.de

How To Cite: Horiachyi, D.O.; Nestoklon, M.O.; Akimov, I.A.; et al. Structural Phase Transitions in Double Perovskite Crystals Studied by Brillouin Light Scattering. *Materials and Sustainability* **2026**, *2*(1), 3. https://doi.org/10.53941/matsus.2026.100003

Received: 9 January 2026
Revised: 2 March 2026
Accepted: 11 March 2026
Published: 24 March 2026

Abstract: Inorganic lead-free double perovskites attract particular interest as a non-toxic and stable material platform for optoelectronic applications. Here, Brillouin light scattering spectroscopy is employed to investigate the elastic properties and structural phase transitions in single crystals of $Cs_2AgBiBr_6$ and $Cs_2AgBiCl_6$. The complete set of elastic constants is evaluated from the Brillouin scattering measurements performed along three different crystallographic directions. Both materials have similar elastic constants and weak elastic anisotropy in the cubic phase. At low temperatures, the lifting of degeneracy of transverse acoustic phonon modes is attributed to a lowering of crystal symmetry. From the temperature dependence of the acoustic phonon frequencies, we determine the structural phase transition temperature of about 43 K for $Cs_2AgBiCl_6$, compared to 122 K in $Cs_2AgBiBr_6$.

Keywords: double perovksite; Brillouin light scattering; structural phase transition; elastic constants

1. Introduction

In recent years great interest to metal halide perovskites has grown rapidly due to the success in photovoltaic applications. The impressive results with power conversion efficiency of lead halide perovskites exceeded 26% thanks to improving the device fabrication routines and the proper choice of atomic elements and their composition in perovskite material [1,2]. The most intensively studied materials are lead halide perovskites with the general formula $APbX_3$, where A is an organic (MA: $CH_3NH_3^+$, FA: $H_2NCHNH_2^+$) or inorganic cation (Cs^+) and X is a halide anion (I, Br, or Cl). The variety of perovskite semiconductors is very wide and is not limited to the lead-based perovskites. Lead can be replaced by other divalent metals such as Sn and Ge. Moreover, a new class of lead-free double perovskite semiconductors with the general formula $A_2B'B''X_6$ with B′ and B″ being monovalent and trivalent metal ions attracted significant attention due to higher stability and lower toxicity [3,4].

Halide perovskites, as semiconductor materials, are of particular interest for fundamental research due to the strong interaction of charge carriers with the lattice, which gives rise to pronounced peculiarities in their electronic, optical, and elastic properties [5]. Photoacoustic studies are of special interest in this context: strain can modify the band gap and exciton energies, while optical excitation with femtosecond pulses can induce coherent lattice vibrations [6–8]. Perovskites provide an appealing platform for such studies due to their rich phase diagram, soft acoustic phonons, and tunable excitonic properties [9–12]. Moreover, efficient generation of high-frequency sub-THz coherent acoustic phonons enables ultrafast control of optical and electronic properties, as studied using femtosecond pump–probe spectroscopy, opening new opportunities for halide perovskites in hypersonics [13–15]. In particular, recent studies demonstrated that efficient generation of transverse acoustic phonons in the double $Cs_2AgBiBr_6$ perovskite occurs due to anisotropic photostriction in the low-temperature tetragonal phase [16]. In this respect, knowledge of the elastic constants of various halide perovskites and their temperature dependence is crucial for photoacoustic studies.

Brillouin light scattering (BLS) spectroscopy is a powerful tool that has been applied, together with inelastic neutron scattering, for the evaluation of elastic softness in a wide range of lead halide perovskites [17]. BLS has also been applied to the $Cs_2AgBiBr_6$ crystals, which are among the most extensively studied double perovskites. The elastic constants of this material have been evaluated using both nanoindentation and BLS spectroscopies [18,19]. However, most studies have been performed at room temperature and for the cubic phase, despite the fact that BLS is highly effective for monitoring structural phase transitions through the temperature dependence of the acoustic phonon energies [16]. Other double perovskites, such as $Cs_2AgBiCl_6$, are far less studied [19,20].

In this study, we investigate the double perovskite semiconductors $Cs_2AgBiBr_6$ and $Cs_2AgBiCl_6$ using BLS spectroscopy. We evaluate and compare the elastic constants of both materials by measuring BLS from different crystallographic facets and at multiple wavelengths. Our results reveal weak anisotropy and a high similarity in the elastic properties of chloride and bromide compounds. At cryogenic temperatures we observe a lowering of cubic symmetry which is manifested in lifting the degeneracy of transverse acoustic phonons. From temperature dependence we determine the structural phase transition temperature to be 43 K in $Cs_2AgBiCl_6$, compared to 122 K in $Cs_2AgBiBr_6$.

2. Methods

2.1. Crystal Growth

The $Cs_2AgBiBr_6$ and $Cs_2AgBiCl_6$ crystals were grown using a controlled cooling crystallization technique in acidic media. High-purity precursors were used without additional purification: cesium bromide (CsBr, 99.999%), cesium chloride (CsCl, 99.9%), silver chloride (AgCl, 99,999%), and bismuth trichloride ($BiCl_3$, 98%) from "Sigma-Aldrich, " (Schnelldorf, Germany); Silver bromide (AgBr, 99%) and bismuth tribromide ($BiBr_3$, 98%) from "Alfa" (Karlsruhe, Germany). As solvents and crystal growth media, hydrobromic acid (HBr, 48%) from "Acros Organics" (Geel, Belgium) and hydrochloric acid (HCl, 36%) from "ThermoScientific" (Dreieich, Germany) were used for $Cs_2AgBiBr_6$ and $Cs_2AgBiCl_6$, respectively. Stoichiometric amounts of the precursors were dissolved in the respective acid by heating the mixture to 120 °C for $Cs_2AgBiBr_6$ and 160 °C for $Cs_2AgBiCl_6$ and maintained at the set temperature for 5 h to ensure complete dissolution. The solution was gradually cooled at a rate of 1 °C per hour to ambient temperature, promoting slow nucleation and crystal growth. The harvested crystals were washed with dichloromethane and dried in air.

2.2. Crystal Characterization

Phase purity and crystal structure were assessed by powder X-ray diffraction (XRD) using a General Electric XRD 3003 TT system equipped with a monochromatic copper (Cu)Kα radiation source. The single crystals were manually pulverized and the resulting powders were uniformly spread onto a low-background polymer holder. Measurements were performed under ambient conditions in Bragg-Brentano geometry within the 10–70 2Θ° range with a step size of 0.005° and an integration time of 5 s per step. The lattice parameters were refined from the indexed reflections assuming the cubic double perovskite structure (space group $Fm\bar{3}m$).

2.3. Brillouin Light Scattering

Brillouin light scattering on $Cs_2AgBiBr_6$ and $Cs_2AgBiCl_6$ crystals was measured using a stabilized multipass double Fabry-Perót Brillouin spectrometer (TFP-2 from Table Stable). The distance between the mirrors was set to 3 mm and the width of the entrance and exit slits was 450 µm. The excitation of the samples was performed with continuous wave (*cw*) single frequency lasers with photon energy of 2.287 eV (542 nm) and 2.407 eV (515 nm) with the spectral width below 40 neV (10 MHz). Microscope objective with 20× magnification and numerical aperture of 0.4 was used for focusing of the excitation laser with intensity of 3 mW into a spot with diameter of about 5 µm. We did not observe any degradation of the sample under excitation at room temperature and at cryogenic temperatures. The scattered light was collected by the same microscope objective in back-scattering geometry. The detection was carried out in the same linear polarization as the excitation laser, such that only vertically polarized light was detected unless stated otherwise in the text. The position of the peaks is independent of the linear polarization direction with respect to crystallographic axes, which excludes possible birefringence. In the analysis of the Brillouin spectra, we assume that the refractive index is a constant independent on the direction. The samples were placed in a helium flow cryostat allowing the temperature dependent measurements from room temperature $T = 293$ K down to 5 K. As-grown bulk single crystals of $Cs_2AgBiCl_6$ and $Cs_2AgBiBr_6$ contain only $\{111\}$ facets. For Brillouin light scattering measurements along different crystallographic orientations, the crystals were subsequently polished to produce surfaces with normals along $\langle 001 \rangle$ and $\langle 110 \rangle$ directions. More details on determination of the crystall direction are discussed in Supplementary Materials.

3. Experimental Results

3.1. Cubic Phase at Room Temperature

It is well established in the literature that $Cs_2AgBiBr_6$ crystals grow along ⟨111⟩ crystallographic directions [21]. The controlled cooling growth yielded millimeter-sized single crystals with well-defined polyhedral shapes with prominent {111} facets for both compounds. $Cs_2AgBiBr_6$ crystals possess orange-red color (Figure 1a), while $Cs_2AgBiCl_6$ crystals have yellow color (Figure 1b), which is related to the increase of the bandgap energy during transition from Br to Cl halide anions [22–24]. The average size of the chloride crystals was about 2 mm, and the bromide crystals were bigger, about 3 mm.

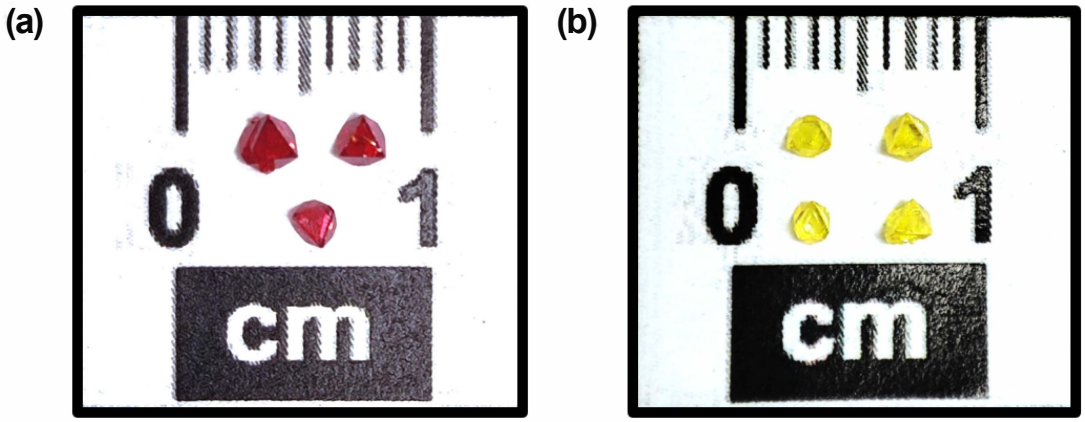

Figure 1. Optical images of (**a**) $Cs_2AgBiBr_6$ and (**b**) $Cs_2AgBiCl_6$ single crystals. The as-grown crystals are bounded solely by {111} facets.

Powder XRD patterns confirmed the formation of a pure cubic double perovskite phase for both materials, with no impurity peaks detected, as shown in Figure 2. Refinement of multiple indexed peaks yielded average lattice constants of $a = 11.29$ Å for $Cs_2AgBiBr_6$ and $a = 10.79$ Å for $Cs_2AgBiCl_6$, which aligns well with data reported in the literature [22,25]. The larger lattice constant in the bromide analog may reflect the greater ionic radius of Br^- (1.96 Å) compared to Cl^- (1.81 Å), which leads to the expanded $[AgX_6]$ and $[BiX_6]$ octahedra.

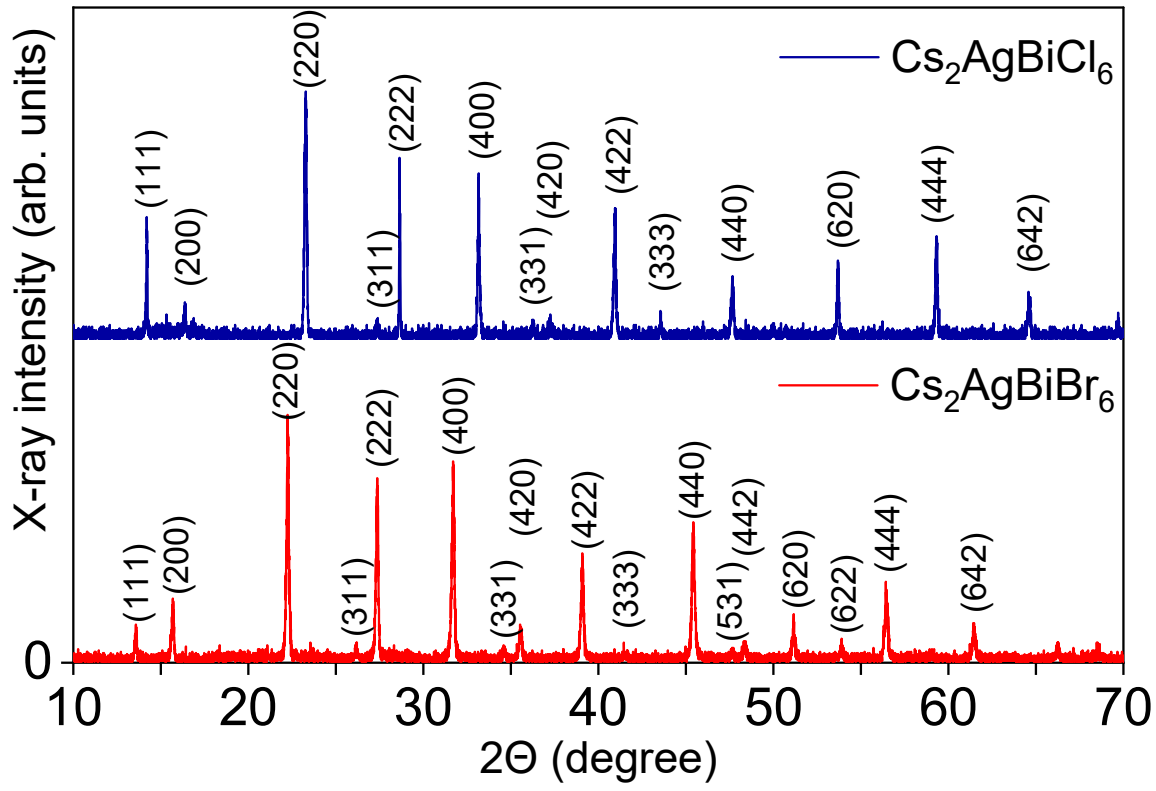

Figure 2. Powder X-ray diffraction patterns of $Cs_2AgBiBr_6$ and $Cs_2AgBiCl_6$ measured at room temperature.

The room temperature BLS data for $Cs_2AgBiCl_6$ and $Cs_2AgBiBr_6$ are summarized in Figures 3 and 4. The BLS spectra comprise one or two narrow peak pairs (Stokes and anti-Stokes) with a spectral width of 0.5 GHz, which is limited by the spectral resolution of the setup. The lower energy peak centered at about 11 GHz is attributed to light scattering with emission or absorption of transverse acoustic (TA) phonon, while the higher energy peak around 22 GHz corresponds to scattering on longitudinal acoustic (LA) phonon. Both $Cs_2AgBiCl_6$ and $Cs_2AgBiBr_6$ crystals have the cubic structural phase at room temperature. In this case TA phonons are doubly degenerate and represented by one peak. The spectral positions of the peaks depend on the composition of the double perovskite crystal (chloride vs bromide), excitation wavelength, and orientation of the crystals. The TA phonons are not active in isotropic case in back-scattering geometry due to symmetry. However, in a cubic crystal structure it is possible to observe TA phonons along $\langle 111 \rangle$ crystallographic direction. For a cubic structure there are three independent optoelastic constants: p_{11}, p_{12} and p_{44}. If the relation $p_{11} = p_{12} + 2p_{44}$ does not hold (i.e., if optoelastic constants are anisotropic), TA phonon is active and can be measured in the backscattering geometry (see table Xlll in ref. [26]).

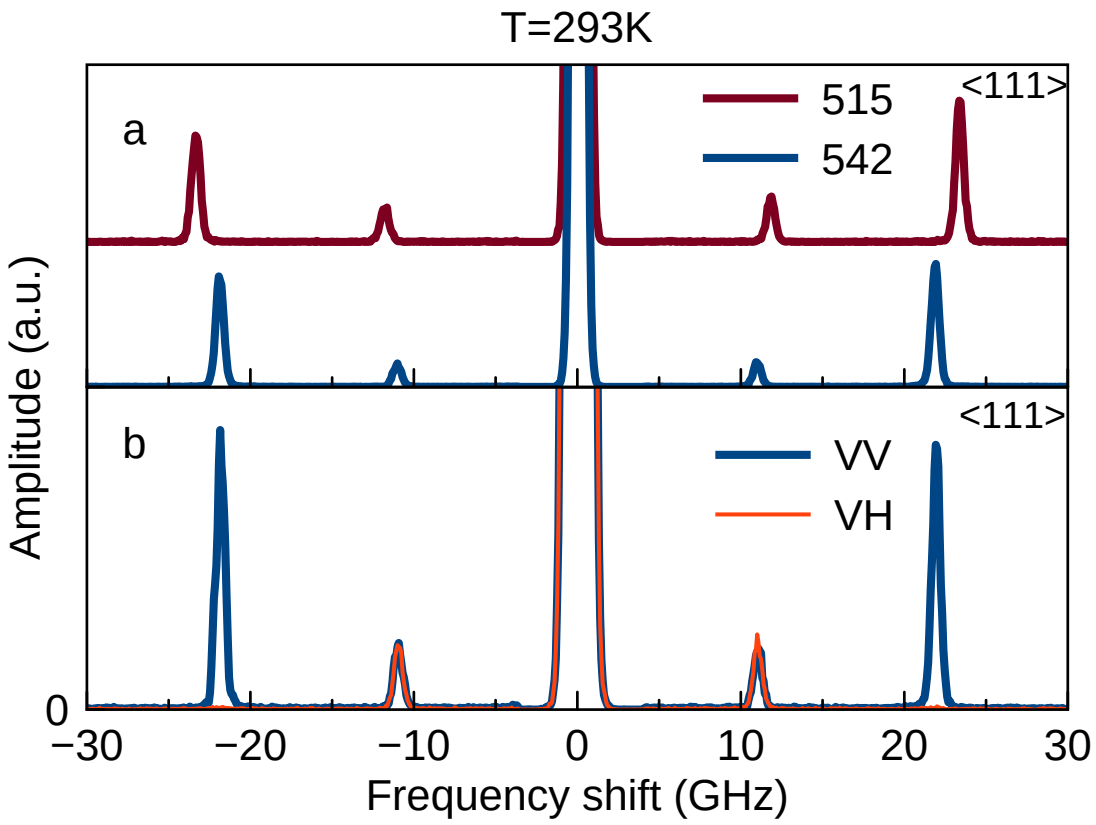

Figure 3. Brillouin light scattering (BLS) spectra measured at room temperature for $Cs_2AgBiCl_6$. (**a**) Excitation with 542 nm (blue) and 515 nm (brown) of $Cs_2AgBiCl_6$ along $\langle 111 \rangle$ crystalographic axis. (**b**) BLS spectra under excitation with 542 nm laser in $Cs_2AgBiCl_6$ in copolarized detection and excitation scheme (VV, blue) and crosspolarized (VH, red).

BLS spectra in $Cs_2AgBiCl_6$ for excitation with different laser lines of 542 and 515 nm are shown in Figure 3a. The data correspond to excitation along $\langle 111 \rangle$ crystallographic direction. In both cases we observe scattering on both TA and LA phonons. For the 542 nm laser we observe two peaks with frequencies of 21.88 GHz and 11.01 GHz, while for the 515 nm laser the BLS peaks shift to higher frequencies, i.e. for longitudinal acoustic phonon to 23.34 GHz and for transverse acoustic phonons to 11.80 GHz, respectively. This change is expected due to momentum conservation. The position of the peak is defined by the acoustic phonon velocity, which is constant near the center of the Brillouin zone. In the back-scattering geometry, the velocity of the s-th mode can be calculated from the peak in the BLS spectrum frequency $\delta\nu_s$ as:

$$V_s = \frac{\lambda}{2n_r}\delta\nu_s. \tag{1}$$

Here, λ is the excitation wavelength and n_r is the refractive index of material. For $Cs_2AgBiBr_6$ refractive index at $\lambda = 542$ nm is 2.17 and at $\lambda = 515$ nm is 2.21 [27]. For $Cs_2AgBiCl_6$, we use 1.91 and 1.95 for these two

wavelengths. We set the refractive index at larger wavelength to the value from Figure 3b in Ref. [24] and their ratio to satisfy Equation (1).

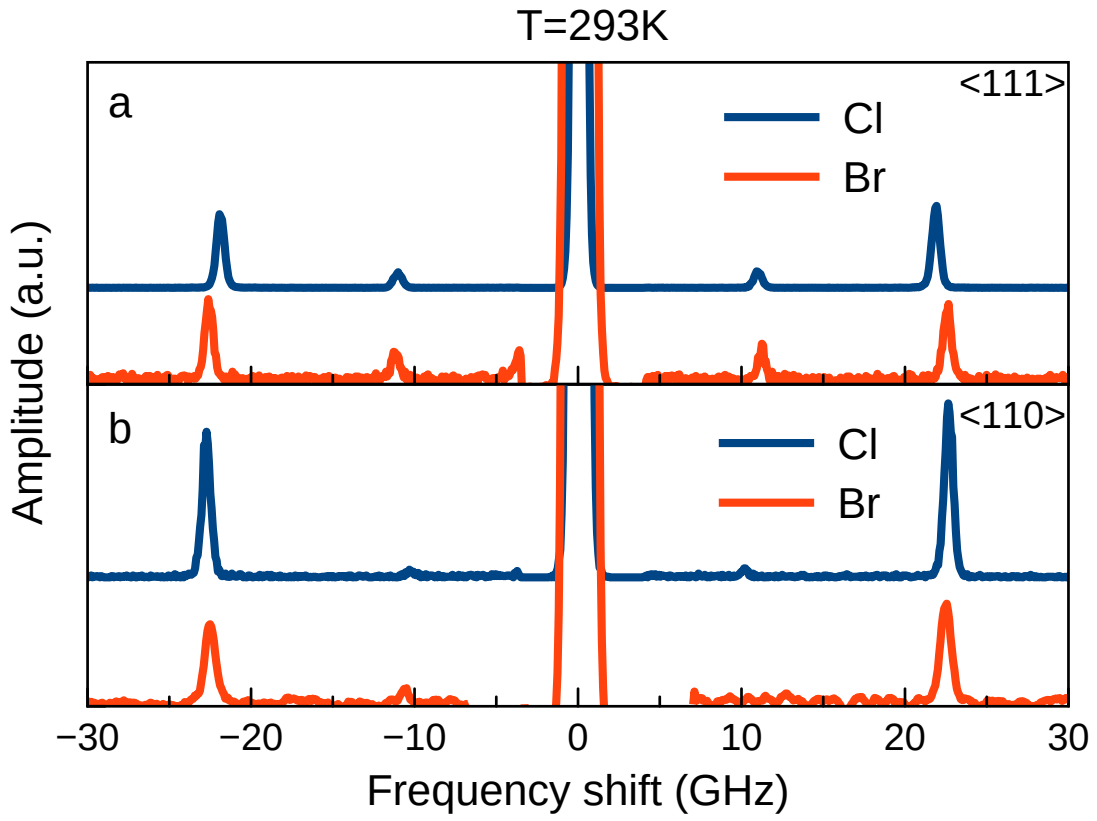

Figure 4. BLS spectra under excitation with 542 nm laser in $Cs_2AgBiCl_6$ (blue) and $Cs_2AgBiBr_6$ (red) measured at room temperature. The data are shown in (**a**,**b**) for excitation along $\langle 111 \rangle$ and $\langle 110 \rangle$ crystallographic directions, respectively.

The BLS spectra measured in copolarized VV and crosspolarized VH configurations are presented in Figure 3b. It follows that the signal corresponding to LA phonons vanishes in VH polarization, while TA phonons are present in both VV and VH configurations. The intensity of Brillouin scattering is given by

$$I \propto \left| e_{2,i}^{T} \, B_{ij} \, e_{1,j} \right|^2 \tag{2}$$

with

$$B_{ij} = p_{ijkl} u_k Q_l, \tag{3}$$

where p_{ijkl} is the tensor of the photoelastic constants, u_k is a phonon amplitude vector, Q_l is a phonon wavevector, $\mathbf{e}_{1,j}$, $\mathbf{e}_{2,i}$ are polarization vectors of incident and scattered light, respectively [26].

Using Equation (2) we obtain that for excitation along $\langle 111 \rangle$ direction in cubic crystal, the intensity of BLS signal from LA phonon in VV polarization configuration is proportional to $p_{11} + 2p_{12} - p_{44}$, whereas in the VH scheme it vanishes. Thus, no LA phonon signal is expected in the cross-polarized detection scheme. For TA phonons the amplitude in VV scheme is proportional to $p_{11} - p_{12} - 2p_{44}$ while in the VH scheme it is proportional to $p_{11} - p_{12} - p_{44}$, which is generaly nonzero. Consequently, TA phonons can contribute to the cross-polarized signal and can be observed in both VV and VH schemes. In what follows we use co-polarized configuration, which allows us to measure all peaks related to LA nad TA modes simultaneously.

Comparison of BLS spectra in $Cs_2AgBiCl_6$ and $Cs_2AgBiBr_6$ under excitation with the same laser (542 nm) along $\langle 111 \rangle$ and $\langle 110 \rangle$ crystallographic directions is presented in Figure 4a,b, respectively. Similar to $Cs_2AgBiCl_6$, in $Cs_2AgBiBr_6$ we observe two peaks with larger frequency shifts of 22.57 GHz and 11.20 GHz along $\langle 111 \rangle$ crystallographic direction. For excitation along $\langle 110 \rangle$ crystallographic direction we observe only one LA peak for chloride and bromide crystals with frequencies of 22.71 GHz and 22.50 GHz, respectively. A weak signature of a signal at 10.2 GHz is related with TA phonon scattering, due to possible aperture broadening and small deviations from normal laser incidence. The data with phonon scattering frequencies $\delta\nu_s$, measured for different

crystallographic directions and corresponding to BLS performed at 542 nm are summarized in Table 1. It follows that the relative position of peak maxima for $Cs_2AgBiCl_6$ and $Cs_2AgBiBr_6$ measured along different crystallographic directions is close to each other. As shown below, since both the density and the value of refractive index are smaller with their ratio almost equal between materials, in $Cs_2AgBiCl_6$, the similar positions of BLS peaks indicate similar values of the elastic constants for both materials.

Table 1. Phonon frequencies evaluated from peak positions in BLS spectra under excitation along different crystallographic directions at room temperature in cubic phase and at 5 K in tetragonal phase under 542 nm laser excitation.

Crystal Facet	Acoustic Phonon	Phonon Frequency (GHz) for $Cs_2AgBiBr_6$	Phonon Frequency (GHz) for $Cs_2AgBiCl_6$
		Cubic phase	
$\mathcal{S}_2$ {100}	LA	22.82	22.70
$\mathcal{S}_1$ {110}	LA	22.50	22.71
$\mathcal{S}_0$ {111}	LA	22.57	21.88
	TA	11.20	11.01
		Low symmetry phase	
$\mathcal{S}_2$	LA	25.37	24.83
$\mathcal{S}_1$	LA	23.34	24.77
	TA_1	13.79	10.72
	TA_2	12.10	7.86
$\mathcal{S}_0$	LA	22.80	22.22
	TA_1	12.17	12.15
	TA_2	10.33	10.86

The spectral position of the Brillouin peaks can be directly related to the components of the elastic stiffness tensor, see details in Appendix A. In particular, c_{11} can be directly calculated from the frequency of LA phonon measured at {001} surface while its change for other surfaces is defined by the $c_{44} - (c_{11} - c_{12})/2$ characterizing the deviation of elastic properties of cubic material from the isotropic one. From the experimental data, we conclude that both materials can be treated as isotropic with a good precision, which is beyond actual experimental resolution. The exact numbers will be discussed below.

The BLS data along different crystallographic directions provide full information about the elastic properties of the material. From the results shown in Table 1, we determine the elastic tensors of the perovskite crystals under study. For the cubic phase, all three components of the elastic tensor are calculated directly from the peak positions. In particular, the position of single LA phonon peak at {001} surface is recalculated to c_{11} as:

$$c_{11} = \frac{\rho\lambda^2}{4n_r^2}\left(\delta\nu_{LA,001}\right)^2 . \tag{4}$$

Other components can be calculated analogously. Note, that in the cubic phase TA phonon modes contribute to the Brillouin signal only at {111} surface. Here, we use the following procedure. We calculate all three constants from the signal at {001} and {111} surfaces and estimate the experimental error by comparing signals at different wavelengths and {110} surface.

For $Cs_2AgBiBr_6$ we obtain $c_{11} = 40.2 \pm 0.3$ GPa, $c_{44} = 10.1 \pm 0.3$ GPa, $c_{12} = 19.4 \pm 0.3$ GPa. Here, the quoted $\pm$ values reflect the estimated accuracy of the extracted constants, inferred from the fact that the peak from {110} facet is shifted by about 0.2 GHz from its expected position. These results are in reasonable agreement with experimental data obtained by nanoindentation and inelastic X-ray scattering in Ref. [18] and density functional theory (DFT) calculations in Ref. [16], see Table 2. Using the same procedure we evaluate the following constants for $Cs_2AgBiCl_6$: $c_{11} = 42.8 \pm 1$ GPa, $c_{12} = 21.2 \pm 1$ GPa, $c_{44} = 8.55 \pm 1$ GPa. Although the uncertainty is somewhat larger in this case, it remains within the resolution of the setup, corresponding to a peak-position accuracy of about ± 0.5 GHz. From determined constants we can calculate the frequencies of all phonons, including the ones which do not contribute to the Brillouin scattering. For ⟨110⟩ direction phonon frequencies should be 10.15 GHz and 11.4 GHz. In Figure 4b we observe small signal with a frequency of 10.2 GHz, which coincides within experimental

accuracy with one of the frequencies expected for TA modes.

Table 2. Elastic constants for $Cs_2AgBiBr_6$ and $Cs_2AgBiCl_6$ from different sources and evaluated from current BLS data. All values are given in GPa.

	Reference	c_{11}	c_{44}	c_{12}
$Cs_2AgBiBr_6$:				
Ref. [18]	Experiment	44.5	8.6	17.6
Ref. [16]	Theory	45.7	7.0	17.2
Ref. [19]	Theory	33.6	7.25	14.5
this work	Experiment	40.2	10.1	19.4
$Cs_2AgBiCl_6$:				
Ref. [19]	Theory	42.1	9.01	15.1
this work	Experiment	42.8	8.55	21.2

3.2. Tetragonal Phase at Low Temperature

At cryogenic temperatures, $Cs_2AgBiBr_6$ is known to have low symmetry crystallographic phase. Below 120 K, it is in the tetragonal phase with #87 space group [10]. There are recent reports that at a temperature of 39 K another structural transition from tetragonal to monoclinic or triclinic phase takes place [28,29]. The latter is not accompanied by a significant change of acoustic properties [16] and below we will assume that the material has the tetragonal phase. The crystallographic directions after the cubic-to-tetragonal phase transition are ambiguous and extra work is needed to identify them. In the cubic phase we identified the surfaces normal to the corresponding crystallographic directions: $\langle 001 \rangle$, $\langle 110 \rangle$, and $\langle 111 \rangle$. To avoid confusion, for these surfaces in the tetragonal phase we will use correspondingly $\mathcal{S}_2$, $\mathcal{S}_1$, $\mathcal{S}_0$.

Figure 5 summarizes the BLS data obtained at low temperature $T = 5$ K for two different facets. The spectrum measured at $\mathcal{S}_0$ surface of $Cs_2AgBiCl_6$ (see Figure 5a) show three peaks with maxima at 22.22 GHz, 12.15 GHz and 10.86 GHz, that are attributed to one longitudinal phonon and two transverse phonons (TA_1 and TA_2), respectively. For $Cs_2AgBiBr_6$ under the same conditions, we observe LA, TA_1, and TA_2 peaks with a frequencies of 22.80 GHz, 12.17 GHz and 10.33 GHz, respectively, see also Table 2.

The presence of three peaks at $T = 5$ K at $\mathcal{S}_0$ surface (see Figure 5a) in case of $Cs_2AgBiBr_6$ is attributed to the transition to a lower symmetry crystal phase. In tetragonal phase the degeneracy of shear acoustic phonons is lifted and we can observe two transverse acoustic phonons with different frequencies. To the best of our knowledge, there is no information about structural phase transitions for $Cs_2AgBiCl_6$. Splitting of transverse acoustic phonons means that the symmetry of the crystal is lowered compared to the one at room temperature. By analogy with other halide perovskite crystals, we suggest that the chloride crystal undergoes a structural phase transition. Note, that the alignment of c-axis along one of the three possible directions in tetragonal phase is not important for the evaluation of peak positions measured at $\mathcal{S}_0$ surface.

Spectra obtained at 5 K at the $\mathcal{S}_1$ surface also show three different peaks in both samples, compared to one peak measured at room temperature. For $Cs_2AgBiBr_6$ peak frequencies are 23.34 GHz, 13.79 GHz and 12.10 GHz, while for $Cs_2AgBiCl_6$ the corresponding frequencies are 24.77 GHz, 10.72 GHz and 7.86 GHz. Here, we observe very strong variation of phonon frequencies, particularly for TA modes, when comparing bromide and chloride samples. Such a big difference in phonon frequencies could be attributed to the fact that in a low symmetry crystal the directions of the cubic phase normal to $\mathcal{S}_1$ surface are no longer equivalent. Therefore, the elastic properties depend on the alignment of c-axis in low symmetry phase and can differ significantly along these directions. In other words, spectra presented in Figure 5b are likely obtained from crystal surfaces that are equivalent in cubic phases and not equivalent in tetragonal phase.

In contrast to the cubic phase, the amount of BLS data in tetragonal phase are not enough to extract all elastic constants, since their number increases from three to seven, especially taking into account the experimental uncertainties in the peaks positions. To compare the values of elastic constants in low symmetry phase one requires larger series of measurements along other crystallographic directions. However, as observed for the cubic phase of both materials, similar peak positions obtained along $\langle 111 \rangle$ direction correspond to close values of the elastic tensor components and we expect to have similar values for elastic constants in low symmetry crystallographic phase.

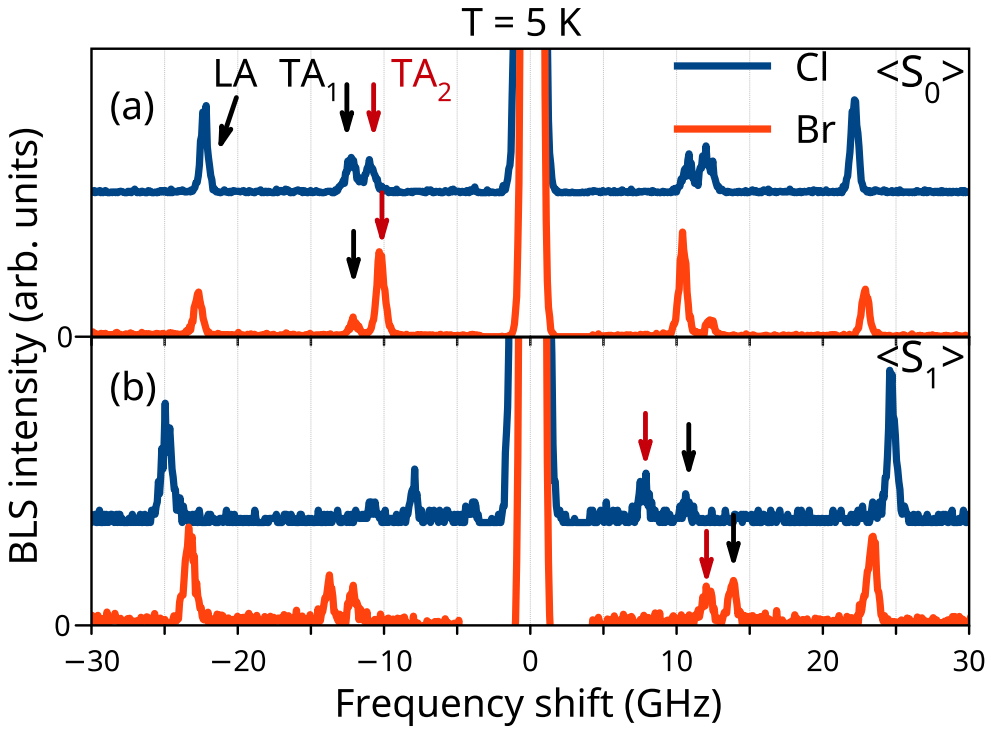

Figure 5. Low temperature BLS spectra at $T = 5$ K. BLS spectra under excitation with 542 nm laser for $Cs_2AgBiCl_6$ (blue) and $Cs_2AgBiBr_6$ (red) measured for $\mathcal{S}_0$ (**a**) and $\mathcal{S}_1$ (**b**) surfaces.

3.3. Temperature Dependence

In order to determine the temperature of structural phase transition phase T_C in $Cs_2AgBiCl_6$ we study the temperature dependence of BLS spectra for $\mathcal{S}_0$ surface. In this case the scattering on all acoustic phonons is well pronounced and positions of the peaks do not depend on the particular alignment of c-axis. The results are summarized in Figure 6. The spectra at selected temperatures are shown in Figure 6a. We observe that an increase in temperature leads to a shift of the TA phonon peaks toward lower frequencies. This effect is particularly pronounced for the TA_2 peak, which becomes very weak and broad at a temperature of 42 K (see spectrum with the TA_1 and TA_2 peaks labeled by black and red arrows, respectively). A further increase in the temperature leads to transformation of two TA peaks into a single TA peak at a higher frequency. It is also worth to note, that linewidth of TA_2 peak undergoes abrupt broadening close to 43 K (see Figure S2). Above 43 K the BLS spectra comprise only two peaks with frequencies corresponding to LA and TA phonons as observed at room temperature in Figure 6b. Therefore, we conclude that in $Cs_2AgBiCl_6$ the structural phase transition between low temperature tetragonal and high temperature cubic phases takes place at $T_C = 43$ K.

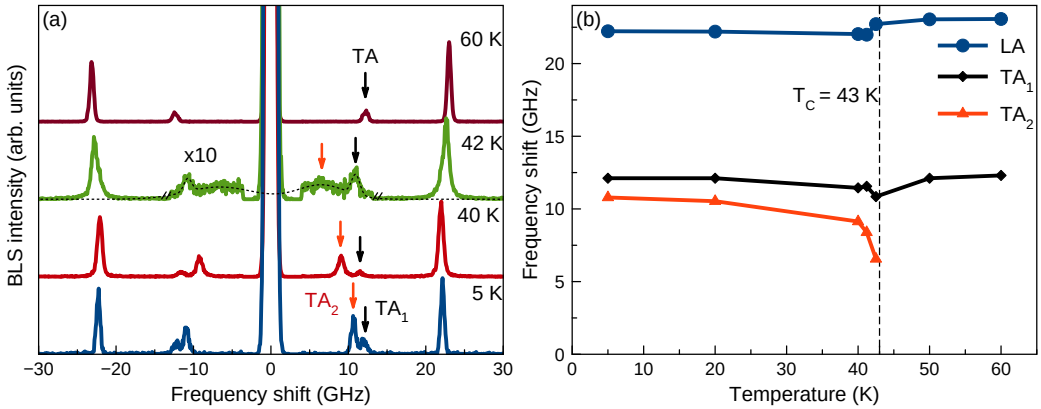

Figure 6. Temperature dependence of the phonon frequencies in $Cs_2AgBiCl_6$ along $\langle 111 \rangle$ crystallographic direction under excitation with 542 nm laser. (**a**) BLS spectra measured at different temperatures. (**b**) BLS peak positions as a function of temperature. Blue points correspond to LA phonons, black - TA_1 phonons in low symmetry crystall structure and TA in cubic phase, red - TA_2 phonons.

The temperature dependence of the peak positions is shown in Figure 6b. Maximum of LA phonon in $Cs_2AgBiCl_6$ shifts by about 0.8 GHz from 22.22 GHz before the phase transition to 23.07 after the phase transition, while TA_1 shifts from 12.11 GHz at 5 K to 12.38 in a cubic phase at 60 K. TA_2 frequency changes from 10.79 GHz to up to 6.50 GHz at 42 K. We emphasize that close to T_C in tetragonal phase we observe a very strong frequency shift of TA_2 mode to lower energies with increasing the temperature. The softening of transverse acoustic modes across the tetragonal–cubic transition has been discussed for $SrTiO_3$ in Refs. [30,31]. We note that the temperature dependence of LA, TA_1 and TA_2 peak positions is very similar to that observed for $Cs_2AgBiBr_6$ as reported in Ref. [16]. However, the temperature of phase transition is lowered from 122 K to about 43 K. It is worth to mention that local heating of the sample in the excitation area may lead to local increase of temperature. Therefore, we keep this value as a lower estimate, meaning that the real T_C could be several degrees larger than 43 K.

4. Discussion

A complete set of experimentally measured elastic properties and phase transition temperature for the lead-free double perovskite $Cs_2AgBiBr_6$ in the cubic phase, where the elastic constants were determined using nanoindentation and inelastic X-ray scattering is availible in the literature [10,18]. To our knowledge, no experimental data on the elastic constants of $Cs_2AgBiCl_6$ have been reported. For this crystal, the BLS spectra are available only along the $\langle 111 \rangle$ crystallographic direction, which is insufficient to determine the complete set of elastic constants [19]. Moreover, the sound velocities along $\langle 111 \rangle$ were obtained using refractive indices derived from DFT calculations. In the present work, by evaluating and comparing BLS data obtained from three different crystal facets, we were able to determine the full set of elastic constants in the cubic phase (see Table 2). We emphasize that these values are very similar for both the bromide and chloride compounds in the cubic phase.

Next, we compare the elastic constants listed in Table 2 with previously reported data for organic lead halide perovskites obtained using inelastic neutron scattering and BLS in Ref. [17]. First, similarly to lead halides the value for c_{11} decreases with the increase of crystal lattice constant, i.e. it is larger for bromide compared to chloride double perovskite. Second, in lead-halides the longitudinal/transverse ratio c_{11}/c_{44} is large (about 10), whereas in double perovskites it is significantly smaller, being about 4. Third, the Zener anisotropy parameter $A = 2c_{44}/(c_{11} - c_{12})$ equals to 0.97 in $Cs_2AgBiBr_6$ and 0.79 in $Cs_2AgBiCl_6$, respectively. This anisotropy is substantially smaller than in lead halide perovskites, where A deviates from unity being in the range 0.3–0.5 [17].

From analysis of temperature dependent BLS data, we conclude that similarly to $Cs_2AgBiBr_6$, the chloride perovskite shows a clear structural phase transition accompanied by the softening of the low frequency TA mode. Compared to $Cs_2AgBiBr_6$, the phase transition in $Cs_2AgBiCl_6$ occurs at lower temperature. Similar behavior was reported for $MAPbBr_3$ and $MAPbCl_3$ crystals (T_C = 237 K and 179 K respectively) [32].

5. Conclusions

We experimentally determine the full set of elastic constants in $Cs_2AgBiBr_6$ and $Cs_2AgBiCl_6$ in cubic phase. In $Cs_2AgBiCl_6$, a phase transition from the cubic phase to a lower-symmetry crystal structure is observed at 43 K, manifested by the splitting of transverse acoustic modes and a pronounced softening of a low-frequency mode. Double perovskites demonstrate a smaller longitudinal/transverse ratio and a smaller degree of anisotropy as compared with lead halide perovskites. Further measurements of multiple facets in combination with polarization resolved studies would allow access to a larger set of elastic constants in the low-temperature phase and enable a more detailed characterization of the elastic anisotropy.

Supplementary Materials

The following supporting information can be downloaded at: https://media.sciltp.com/articles/others/260324112614387 7/MatSus-26010041-Supplementary_Materials.pdf, Section S1: Density; Section S2: Determination of crystall directions; Figure S1: Photo of a polished sample $Cs_2AgBiBr_6$ with $\langle 001 \rangle$, $\langle 110 \rangle$ and $\langle 111 \rangle$ crystallographic directions; Figure S2: Full width at half maximum of Brillouin peaks corresponding to scattering on TA and LA phonons as a function of temperature in $Cs_2AgBiCl_6$ measured along $\langle 111 \rangle$ crystallographic direction at room temperature.

Author Contributions

D.O.H. performed the measurements. I.A.A. and D.O.H. analyzed the data. M.O.N. developed the theoretical approach. V.V., O.T., and V.D. grew the samples and performed XRD. All authors contributed to interpretation and analysis of the data. D.O.H., I.A.A., and M.O.N. wrote the manuscript in close consultations with M.B., D.R.Y., and V.D. All authors have read and agreed to the published version of the manuscript.

Funding

The Dortmund and Würzburg groups acknowledge financial support from the Deutsche Forschungsgemeinschaft within the SPP 2196 (project no. 506623857). D.O.H. acknowledges the Deutsche Forschungsgemeinschaft (project no. 536987509). V.V. acknowledges financial support from DFG Würzburg-Dresden Cluster of Excellence on Complexity, Topology and Dynamics in Quantum Matter – ctd.qmat (EXC 2147, project-id 39085490).

Data Availability Statement

The data that support the findings of this study are available from the corresponding author upon reasonable request.

Acknowledgments

The authors thank Dirk Schemionek for polishing of the crystals.

Conflicts of Interest

The authors declare no conflict of interest.

Use of AI and AI-Assisted Technologies

No AI tools were utilized for this paper.

Appendix A. Acoustic Phonons Velocities

The velocities of the acoustic phonon modes V_s are the eigenvalues of the equation

$$\left(\rho V_s^2 \delta_{il} - c_{ijkl} Q_j Q_k\right) U_l = 0\,, \tag{A1}$$

where ρ is the density of material, c_{ijkl} are elastic constants of the material and $\mathbf{Q}$ is the direction of the phonon wave vector, δ_{il} is a Kronecker symbol.

In cubic material, there are three independent components of the elastic tensor denoted as c_{11}, c_{44} and c_{12}. For the analysis, it is more convenient to use c_{11} and c_{44} which are directly connected with sound velocities of isotropic material and $c_{\delta c} = c_{44} - (c_{11} - c_{12})/2$, which characterizes the anisotropy of the material and related with Zener anisotropy index [33] $A = 2c_{44}/(c_{11} - c_{12})$ as $c_{\delta c} = c_{44}(1 - 1/A)$. In isotropic material, $A = 1$ and $c_{\delta c} = 0$. With these notations, from Equation (A1) it is easy to find (c.f. Table XIII in Ref. [26]) velocities for the wave vector along high symmetry directions:

$$\mathbf{Q}\|[001]: \qquad \rho V_{TA}^2 = c_{44}\,, \qquad \rho V_{LA}^2 = c_{11}\,; \tag{A2}$$

$$\mathbf{Q}\|[110]: \qquad \rho V_{TA1}^2 = c_{44}\,, \qquad \rho V_{TA2}^2 = c_{44} - c_{\delta c}\,, \tag{A3}$$

$$\rho V_{LA}^2 = c_{11} + c_{\delta c}\,;$$

$$\mathbf{Q}\|[111]: \qquad \rho V_{TA}^2 = c_{44} - \frac{2}{3} c_{\delta c}\,, \tag{A4}$$

$$\rho V_{LA}^2 = c_{11} + \frac{4}{3} c_{\delta c}\,.$$

References

1. Jia, Z.; Guo, X.; Yin, X.; et al. Efficient near-infrared harvesting in perovskite–organic tandem solar cells. *Nature* **2025**, *643*, 104–110.
2. Schmidt-Mende, L.; Dyakonov, V.; Olthof, S.; et al. Roadmap on organic–inorganic hybrid perovskite semiconductors and devices. *Apl Mater.* **2021**, *9*, 109202.
3. Tress, W.; Sirtl, M.T. $Cs_2AgBiBr_6$ Double Perovskites as Lead-Free Alternatives for Perovskite Solar Cells? *Sol. RRL* **2022**, *6*, 2100770.
4. Zhang, Z.; Sun, Q.; Lu, Y.; et al. Hydrogenated $Cs_2AgBiBr_6$ for significantly improved efficiency of lead-free inorganic double perovskite solar cell. *Nat. Commun.* **2022**, *13*, 3397.
5. Yamada, Y.; Kanemitsu, Y. Electron-phonon interactions in halide perovskites. *NPG Asia Mater.* **2022**, *14*, 48.
6. Thomsen, C.; Grahn, H.T.; Maris, H.J.; et al. Surface generation and detection of phonons by picosecond light pulses. *Phys. Rev. B* **1986**, *34*, 4129–4138.
7. Young, E.S.K.; Akimov, A.V.; Campion, R.P.; et al. Picosecond strain pulses generated by a supersonically expanding electron-hole plasma in GaAs. *Phys. Rev. B* **2012**, *86*, 155207.

8. Ruello, P.; Gusev, V.E. Physical mechanisms of coherent acoustic phonons generation by ultrafast laser action. *Ultrasonics* **2015**, *56*, 21–35.
9. Dougherty, T.P.; Wiederrecht, G.P.; Nelson, K.A.; et al. Femtosecond time-resolved spectroscopy of soft modes in structural phase transitions of perovskites. *Phys. Rev. B* **1994**, *50*, 8996–9019.
10. Schade, L.; Wright, A.D.; Johnson, R.D.; et al. Structural and Optical Properties of $Cs_2AgBiBr_6$ Double Perovskite. *ACS Energy Lett.* **2019**, *4*, 299.
11. Steele, J.A.; Lai, M.; Zhang, Y.; et al. Phase Transitions and Anion Exchange in All-Inorganic Halide Perovskites. *Accounts Mater. Res.* **2020**, *1*, 3–15.
12. Kirstein, E.; Yakovlev, D.R.; Glazov, M.M.; et al. The Landé factors of electrons and holes in lead halide perovskites: universal dependence on the band gap. *Nat. Commun.* **2022**, *13*, 3062.
13. Lejman, M.; Vaudel, G.; Infante, I.C.; et al. Giant ultrafast photo-induced shear strain in ferroelectric $BiFeO_3$. *Nat. Commun.* **2014**, *5*, 4301.
14. Mante, P.A.; Stoumpos, C.C.; Kanatzidis, M.G.; et al. Electron–acoustic phonon coupling in single crystal $CH_3NH_3PbI_3$ perovskites revealed by coherent acoustic phonons. *Nat. Commun.* **2017**, *8*, 14398.
15. Guo, P.; Xia, Y.; Gong, J.; et al. Polar Fluctuations in Metal Halide Perovskites Uncovered by Acoustic Phonon Anomalies. *ACS Energy Lett.* **2017**, *2*, 2463–2469.
16. Horiachyi, D.O.; Nestoklon, M.O.; Akimov, I.A.; et al. Efficient launching of shear phonons in photostrictive halide perovskites. *Sci. Adv.* **2025**, *11*, eadw9172.
17. Ferreira, A.C.; Létoublon, A.; Paofai, S.; et al. Elastic Softness of Hybrid Lead Halide Perovskites. *Phys. Rev. Lett.* **2018**, *121*, 085502.
18. Lun, Y.; Liu, J.; Wei, B.; et al. Elastic Properties of Photovoltaic Single Crystal $Cs_2AgBiBr_6$. *Exp. Mech.* **2022**, *62*, 117–123.
19. Naqvi, F.H.; Ko, J.H.; Kim, T.H.; et al. Vibrational, optical and elastic properties of Cs_2AgBiX_6 (X = Br, Cl) double perovskite materials: DFT, PL, Raman and Brillouin scattering studies. *J. Alloys Compd.* **2025**, *1010*, 176968.
20. Pang, S.; Liu, X.; Luo, J.; et al. Brillouin Light Scattering of Halide Double Perovskite. *Adv. Photonics Res.* **2022**, *3*, 2100222.
21. Su, J.; Huang, Y.Q.; Chen, H.; et al. Solution Growth and Performance Study of Cs2AgBiBr6 Single Crystal. *Cryst. Res. Technol.* **2020**, *55*, 1900222.
22. Gray, M.B.; McClure, E.T.; Woodward, P.M. $Cs_2AgBiBr_{6-x}Cl_x$ solid solutions – band gap engineering with halide double perovskites. *J. Mater. Chem. C* **2019**, *7*, 9686–9689.
23. Zelewski, S.J.; Urban, J.M.; Surrente, A.; et al. Revealing the nature of photoluminescence emission in the metal-halide double perovskite $Cs_2AgBiBr_6$. *J. Mater. Chem. C* **2019**, *7*, 8350–8356.
24. Jain, P.; Tran, M.N.; Cleveland, I.J.; et al. Vapor Deposition and Optical Properties of $Cs_2AgBiCl_6$ Thin Films. *J. Phys. Chem.* **2025**, *129*, 5301–5311.
25. McClure, E.T.; Ball, M.R.; Windl, W.; et al. ChemInform Abstract: Cs_2AgBiX_6 (X: Br, Cl): New Visible Light Absorbing, Lead-Free Halide Perovskite Semiconductors. *ChemInform* **2016**, *47*.
26. Vacher, R.; Boyer, L. Brillouin Scattering: A Tool for the Measurement of Elastic and Photoelastic Constants. *Phys. Rev. B* **1972**, *6*, 639–673.
27. Polyanskiy, M.N. Refractiveindex.info database of optical constants. *Sci. Data* **2024**, *11*, 94.
28. Cohen, A.; Brenner, T.M.; Klarbring, J.; et al. Diverging Expressions of Anharmonicity in Halide Perovskites. *Adv. Mater.* **2022**, *34*, 2107932.
29. Tower, C.; Razavi, F.S.; Dion, J.; et al. Low-temperature structural instabilities of the halide double perovskite $Cs_2AgBiBr_6$ investigated via x-ray diffraction and infrared phonons. *arXiv* **2025**, arXiv:cond-mat.mtrl-sci/2505.10563.
30. Fleury, P.A.; Scott, J.F.; Worlock, J.M. Soft Phonon Modes and the 110°K Phase Transition in $SrTiO_3$. *Phys. Rev. Lett.* **1968**, *21*, 16–19.
31. Hehlen, B.; Arzel, L.; Tagantsev, A.K.; et al. Brillouin-scattering observation of the TA-TO coupling in $SrTiO_3$. *Phys. Rev. B* **1998**, *57*, R13989–R13992.
32. Simenas, M.; Gagor, A.; Banys, J.; et al. Phase Transitions and Dynamics in Mixed Three- and Low-Dimensional Lead Halide Perovskites. *Chem. Rev.* **2024**, *124*, 2281–2326.
33. Zener, C. *Elasticity and Anelasticity of Metals*; Chicago University Committee on Publications in the Physical Sciences, University of Chicago Press: Chicago, IL, USA, 1948.